Numerical simulation of high-order above-threshold-ionization enhancement in argon

H. G. Muller
FOM Institute for Atomic and Molecular Physics, Postbus 41883, 1009 DB Amsterdam, The Netherlands
(Received 19 March 1999)

Resonant enhancement of high-order peaks in the photoelectron spectrum of argon at 800 nm is studied by numerical precision integration of the time-dependent Schrödinger equation in the single-electron approximation. It is shown that electrons in the backscattering region of the spectrum are almost exclusively due to resonances. Wave-function analysis shows that there are two types of resonant states: high-angular-momentum states that stay away from the nucleus and mainly decay by emission of low-energy electrons, and states that are located near the polarization axis. These latter states predominantly decay through violent collision with the ionic core, and are responsible for the enhancement of high-energy photoelectrons. [S1050-2947(99)03708-7]

PACS number(s): 32.80.Rm, 34.50.Rk

I. INTRODUCTION

Photoionization of noble-gas atoms with optical or near-infrared lasers requires so many photons that a measurable rate can only be obtained when the field strength of the electromagnetic wave approaches that of the Coulomb attraction to the nucleus. At such intensities, excited states and continua are completely mixed. As a consequence ionization usually goes accompanied by absorption of a large excess of photons, a process known as above-threshold ionization (ATI) [1].

High-sensitivity experiments with high repetition rate lasers [2,3] have made it possible to study ATI spectra to very high orders. Such studies have revealed that atoms can absorb many times their ionization potential's worth of photons. As simple classical arguments have shown, the low-order part of the ATI spectrum is essentially due to the acceleration of the ejected photoelectron in the electromagnetic field of the ionizing laser [4], an acceleration that results in an oscillatory ''quiver'' motion superimposed on the cycle-average ''drift'' velocity. As such, the low-order ATI spectrum is largely atom independent, the influence of the atom being limited to the production mechanism of the free electron. This ''two-stage'' approach, where the atom is modeled as a source of monochromatic electrons, has done rather well in explaining the shape of low-order ATI spectra.

The time-averaged kinetic energy of the electron due to its quiver motion is known as the ponderomotive potential U_P, and it can exceed the photon energy $\hbar\omega$ many times. In the two-stage model [5], or other models that neglect the interaction of the photoelectron with its parent ion once ionization has been effected [6,7], the ATI spectra do not extend much past energies above $2U_P$, the maximum drift energy that can be acquired by a photoelectron after its release in the field by the original ionization event [4]. The global shape of this low-order part of the spectra does depend on how the production of electrons in the source correlates with the phase of the laser. Concentration of ionization near maxima of the electric field $E(t)$, as expected in the case of tunneling, will (in the case of linear polarization) lead to a dominance of low-energy electrons [8]. On the other hand, a steady production, such as Auger decay, will lead to a more homogeneous distribution over the peaks in the allowed energy interval [9].

The situation is more interesting for high-order ATI. Classically, energies above $2U_P$ (''superponderomotive'' or ''hot'' electrons) can only be acquired through an additional interaction of the photoelectron with its parent ion. Since the quiver velocity is a unique function of time, all momentum transfer during an instantaneous scattering event (i.e., one fast compared to the optical cycle) is taken up by the drift motion. Thus, especially scattering in the backward direction can lead to a large change of the drift velocity, if it happens near a zero crossing of the electric field, when the electrons move fast. The details of the electron-ion scattering interaction are expected to depend strongly on the atomic species, and indeed the high-order part of ATI spectra shows a lot of element-specific structure [10,11].

The envelope of most ATI spectra does not decrease regularly, but shows regions where the peak magnitudes stay roughly constant or even increase with peak order [3]. In analogy with high-harmonic generation [12], these regions have been called plateaus. On closer examination, however, these plateaus do not seem very flat, but look more like enhancements of a couple of ATI peaks around a certain order.

Recent high-resolution experiments have revealed substructure in the ATI peaks of plateaus in argon [10] and xenon [11]. Such substructure in the ponderomotively broadened ATI peaks demonstrates that those plateaus are due to resonant processes, i.e., the production of photoelectrons in that energy region occurs at well defined light intensities, and drops by at least an order of magnitude for intensities only a few percent different.

ATI substructure is well known from resonance-enhanced multiphoton ionization (MPI) at lower intensities [13], where it occurs because excited states are Stark shifted to an energy an integer number of photons above the ground state, to be resonantly populated through a multiphoton transition. The bound-bound transition is usually much stronger than direct ionization, and, once populated, the excited states ionize easily. Such behavior was, however, unexpected at the high intensity 70 TW/cm^2) used in the argon experiment. All excited states there lie very far above and outside the potential barrier created by the combined action of the nuclear Coulomb attraction and the laser field [14]. Under these circum-

stances the electron cannot resist the laser and is driven into a full-blown quiver motion, which (at this intensity) displaces it over a distance $2\alpha_0 \cong 26$ bohrs. Any resonant intermediate state must thus be completely deformed by the laser, its quiver energy far exceeding its binding energy. Yet the narrow width of the individual subpeaks suggests that the involved states must have appreciable lifetimes [10].

In contrast, states involving inner-shell excitations of the Ar^+ core, e.g., $(3s)(3p)^5$ are at least as rigid as the Ar ground state, and suggestions that such excitations might somehow be involved have been put forth [15]. In the current paper, however, two-electron effects are completely neglected. Instead we study the dynamic effects of the interaction between photoelectrons and their parent ion in a single-electron picture. In a previous paper [16] it was shown that electron spectra calculated by numerical solution of the time-dependent Schrödinger equation can show quantitative agreement with the experimental results for the observed argon plateau. In this paper we present a more systematic study of resonance enhancements in the ATI spectrum of argon at 800 nm by the same method.

II. NUMERICAL METHODS

Numerically solving the time-dependent Schrödinger equation to simulate the argon plateau at 800 nm is a computationally demanding problem. The laser frequency is low on the atomic scale (the duration of the optical cycle is about 109 atomic time units), and to allow resonance effects to develop takes many optical cycles. The photoelectrons of interest are rather high in energy, and to contain them on the grid during such a long time requires a grid with a large radial dimension. To accurately represent these fast electrons requires small temporal and spatial grid spacings, driving up the number of grid points even further.

To make the problem tractable at all, it is essential to formulate it in the velocity gauge: At the large distances the electrons reach, instantaneous energies and angular momenta would grow completely out of hand in the length gauge [17]. On the other hand, in the acceleration (Kramers-Henneberger [18]) gauge the displaced nuclear potential would be angle dependent, causing a nonsparse coupling between the various partial waves.

A. The model atom

The atom was treated in the single-active-electron approximation, as a simple potential well. In heavier atoms, the presence of inner shells causes problems due to their rapid time evolution. Using a pseudopotential [19] would solve these problems by eliminating such shells, while exactly preserving the scattering properties of the core for all energies in the valence-shell range and above. Unfortunately, the commonly used pseudopotentials are l dependent. Since p, and thus $l = r \times p$, is not a gauge-independent quantity, the pseudopotential cannot be transformed to the velocity gauge as a local (multiplicative) potential. In the present calculations, this problem was solved by relaxing the requirement that the scattering properties of the model electron-ion interaction be exact up to infinite energy. Instead, highly accurate scattering behavior was only required in the energy range of collisions that will occur in practice, i.e., up to $3.17U_P$ [20].

Since spin-orbit coupling in argon is a relatively minor effect even in the $3p$ ground state (178 meV), the model neglects it completely, and describes the atom as a single non-relativistic electron in a (three-dimensional) potential well

$$V(r) = [1 + Ae^{-Br} + (17 - A)e^{-Cr}]/r. \tag{1}$$

(Atomic units are used unless mentioned differently.) For $A = 5.4$, $B = 1$, $C = 3.682$ the eigenenergies of an electron bound in this potential faithfully reproduce the configuration averages of the binding energies of the singly excited states [21], but of course lack the splitting of levels within one configuration due to angular coupling effects [22]. In addition, the K-shell, L-shell, and $3s$ ionization potentials are reproduced correctly, and $V(r)$ possesses the proper asymptotic behavior for $r \to \infty$ and $r \downarrow 0$. Thus, $V(r)$ can be considered an excellent approximation to the electron-ion interaction (including exchange), as long as core excitations are absent. Due to the deep potential well supporting inner shells, however, Eq. (1) cannot be used as such.

To obtain a potential suitable for the intended simulation, use was made of the fact that the first radial node of the p wave and the second node of the s wave in the potential $V(r)$ nearly coincide. Imposing a hard-core boundary condition $[\Psi(R) = 0]$ on the wave function Ψ near this ''common'' nodal point therefore only induces a minor distortion of these waves, and eliminates the K and L shells. The d wave, however, still penetrates to this point (near $r = 0.47$) and the quantum defect of the d states turns out to be exquisitely sensitive to small distortions of the potential (a property that the model shares with the real atom, as evidenced by the large difference in d-quantum defect due to the minor difference in charge distribution of the $P_{1/2}$ and $P_{3/2}$ core). In addition, the hard-core boundary condition is a little too hard: in the true eigenfunctions the nodes move slightly inward with increasing energy, producing a marked dependence of the quantum defects on energy (again, especially for the d states).

Most of the problems with s- and d-quantum defects could be cured by using a soft repulsive core $W(r)$ instead of a hard sphere. The outward push of this core on the d states (for which no inner shells have to be eliminated) could be compensated by providing an attractive tail to this core,

$$W(r) = F\{[(R_x - r)/G]^5 - [(R_x - r)/G]^4\}. \tag{2}$$

The s and d states are less sensitive to the presence of the attractive tail, since their potential well is still quite deep at the place where this tail occurs. The whole core modification (chosen to be four times differentiable so as not to spoil the accuracy order of the numerical integration method) is confined to the range $R < r < R_x$. With $R_x = 3$, $F = 2.5$, $G = 2.017\,85$ this potential repaired the quantum defects of all s and d states to within 0.01 of the original ones, that of the p states to within 0.04, with an exact representation of the $3p$ energy. Higher angular momenta do not penetrate significantly within R_x (the inner turning point of the threshold f wave is $r = 6$), and remain purely hydrogenic. In the relevant

energy range (-1 to $+1$ hartree) the scattering behavior of $V(r)$ (as determined from the phase shifts) is hardly affected by the repulsive core.

The $3s$ state is not removed by the procedure sketched above. Its binding energy, however, is of the order of the energies that photoelectrons acquire anyway, and so the presence of this state does not put an additional burden on the step sizes. After propagation it was always confirmed that the $3s$ population had remained negligible.

Outside R_x all eigenfunctions in the well $V(r)+W(r)$ are identical to those in $V(r)$, (also in normalization; the proper boundary condition guarantees this) but the differences for $r<R_x$ would slightly alter the matrix elements of $\mathbf{E}\cdot\mathbf{r}$ between those functions. In principle, this could be counteracted by adapting the laser potential inside the core (leaving some scalar potential there after the gauge transformation). For the treated intensities, this modification would be very small. It was found that small potentials inside the classically allowed region of the ground state, varying at the laser frequency, in general have little or no effect on the ionization process: the state simply adapts adiabatically to this through a small perturbation. For this reason, the laser interaction was not corrected at all for the presence of the repulsive core.

B. Time evolution

The time-dependent Schrödinger equation,

$$i\partial_t\Psi=\{-1/2p^2+\mathbf{p}\cdot\mathbf{A}(t)+V(r)+W(r)\}\Psi, \qquad (3)$$

was integrated using a method that was fourth order in the spatial grid spacing Δr, and second order in the temporal spacing Δt. (The Appendix contains a brief overview of this method; for an extensive description of the propagator, see Ref. [23].) At the far end of the grid, an absorbing wall removed photoelectrons that reached that point. The wall was implemented by multiplying after each time step with a mask function $1-(d/60)^4$, where d is the penetration depth into the absorber. No attempt was made to absorb the wave function at the l boundary of the grid, since the number of l states could be chosen large enough to completely contain the wave packet.

An initial $3p$ state oriented along the laser polarization [24] was subjected to an N-cycle laser flat-top laser pulse $A(t)=A_0\hat{z}\cos\omega t$ $(0<t<NT)$, preceded by a half-cycle turn on $A(t)=A_0\hat{z}(0.5\cos\omega t+0.125\cos 2\omega t+0.375)$ and followed by a similar turn off [25]. Switching times were kept as short as possible, to minimize the loss of fast photoelectrons at the end of the grid during it. The switching used is four times differentiable both at $t=0$ and $t=-T/2$ [and on $t=NT$ and $t=(N+1/2)T$], minimizing nonadiabatic shakeup of the tightly bound ground state. Since $A(t)$ returns to zero outside the pulse, the switching does not impart any velocity to free electrons. (They suffer some displacement, though, but this does not affect energy spectra.) Finally, the maximum electric field during switching is only 65% of $E_0=\omega A_0$ in the main part of the pulse, so that a negligible amount of tunnel ionization (as compared to later cycles) takes place during the switching interval.

Due to the absence of spin-orbit splitting, the ionization potential of the model atom is slightly different from that of the real atom. As a consequence, there is a small shift in resonance intensities, that, for optimal comparison with experiments, can be compensated by a shift in wavelength. The photon energy used in all presented calculations was $\omega=0.057\,73$ ($\lambda=789.3$ nm), which makes the 12-photon resonance with an $n=4$ state (which seemed to be the most dominant feature in experimental spectra) occur at the same intensity as such a resonance in the real atom would occur for $\lambda=792.5$ nm (the wavelength used in Ref. [10]).

To economize on computation time, first a number of optical cycles were run on a small grid, just large enough to contain a (quivering) atomic state. This ''leader'' provides time for populating a prospective resonant excited state, and for most turn-on transient effects to decay. After that the grid was continually expanded so as to keep all electrons of interest emitted during the last ten cycles of the pulse on the grid. This procedure also serves to avoid contamination of the electron spectra by electrons from the period during which a resonance developed, and at the same time prevents biasing the calculated spectra in favor of slow electrons that take longer to move off the grid.

C. Convergence

As discussed in Ref. [17], convergence of a numerical simulation is a highly nonuniform matter. Some quantities converge more rapidly than others, and even the convergence of one observable can depend strongly on its numerical value. In principle, the exact value of all calculated quantities can be obtained by taking Δt and Δr to 0 while keeping all other quantities (such as the laser intensity, and the position of the absorbing wall) fixed.

This procedure does not perform very satisfactorily in the presence of very narrow resonances, because a tiny shift of the resonance intensity might produce a completely different (nonresonant versus resonant) electron spectrum [32]. The electron spectrum taken at the intensity that follows the peak of a certain resonance converges much faster than that at a fixed intensity near it.

This remark is important for understanding the accuracy of the calculated results. Ionization rates and instantaneous dipole moments away from resonance are typically converged to better than 0.1% of their typical value at $\Delta r=0.2$ and $\Delta t\approx 0.1$ (1000 steps per cycle). This agrees well with expectations: the leading errors due to spatial and temporal discretization on states with momentum k and energy E are $\frac{1}{240}(k\Delta r)^4$ and $\frac{1}{12}(E\Delta t)^2$, respectively, so the mentioned values should work very well for energies up to 0.5 hartree, in which range the ground state and the dominantly populated excited states all lie. For a calculation without narrow features (e.g., with a temporal $\sin^2$ envelope on the laser pulse, broadening ATI peaks and resonance profiles) these parameters would be completely satisfactory.

The physics of the atomic system is thus very well reproduced; nevertheless, in the high part of the electron spectra the ATI peaks will be shifted a little in energy, although their calculated magnitude is very good. Similarly, the resonances will occur at a slightly different intensity, although the spectrum at a particular resonance is well represented. Getting the high-order ATI peaks exactly (i.e., to within a small fraction of their width) in the right place might easily drive up the required amount of work by a factor 5, mostly wasted effort,

since the peak spacing is known *a priori* to be equal to the photon energy. In fact these energy shifts are a well understood effect of the finite time step [26], that can largely be corrected for, and so we did not try to obtain this correction by purely numerical means.

Due to the velocity-gauge formulation [17,27], only 20 to 30 partial waves were needed to obtain convergence. This is in accordance with a rough estimate: at $E_0=0.07$ tunneling results in a wave packet with a transverse momentum spread $\Delta p=E_0^{3/8}=0.37$, assuming that tunneling is dominated by the lowest transverse mode of the (nearly harmonic) saddle-point potential. The quiver motion displaces this packet with respect to the point from which angular momentum is measured by $2\alpha_0=42$, for a total angular momentum 15. The maximum drift momentum perpendicular to the polarization of a rescattered electron can be around 1 a.u., and the quiver motion displaces the line on which such an electron moves by α_0 to either side, so angular momentum is expected to run up to 20 for electrons escaping in this direction.

At selected intensities convergence was tested by making runs with 40 angular momenta and up to 4000 time steps per cycle. This confirmed that the electron spectra would not change visibly on the scale of the plots by going to smaller time steps or including more angular momenta. Only in the wing of very narrow resonances was the spectrum at fixed intensity sensitive to the temporal step size, but in those cases the changes could be undone by slightly shifting the intensity. A comparison with high-precision experimental spectra confirms that the calculated electron spectra are essentially exact [28].

D. Final-state analysis

After the pulse the wave function that remained on the grid was energy analyzed for each angular-momentum channel l with a fourth-order energy window [29] $\Omega(E)=\gamma^4/[\gamma^4+(E-H^{\rm at})^4]$, using the same atomic Hamiltonian $H^{\rm at}$ as was used in the propagation. At each energy E this gives the yield in the energy band with half-width γ around it as $\langle\Psi|\Omega(E)|\Psi\rangle$. The angle-integrated electron spectrum was obtained by adding the spectra obtained from the individual l waves. The spectrum along the polarization axis was calculated by adding the l components of the filtered wave functions with the phase and amplitude prescribed by the corresponding spherical harmonic, respectively, before calculating their norm. In addition, the electron spectrum of the highest l component was calculated, to check that it was insignificant not only in terms of total population, but also at any energy separately.

For some of the analysis, it was necessary to remove the ground-state population during the pulse. This had to be done with extreme care, because at the intensities studied the amount of ionization can be as low as 1 part in 10^4 per optical cycle, and any shakeup due to imperfect ground-state removal must be kept small compared to that. Orthogonalizing on the (properly gauge transformed) unperturbed ground state Φ_0 fell short of this criterion by several orders of magnitude, even if it was done at a zero crossing of the electric field $E(t)$ where one would expect minimum polarization of the state. A convenient method that performed satisfactorily (at these zero crossings) was to run the time propagation for the turn off, orthogonalize on Φ_0, and then run the turn off backwards. This is equivalent to orthogonalizing on the state that evolves from Φ_0 in the turn on, which, due to the high differentiability and low ionization loss of this turn on, is very close to what is desired.

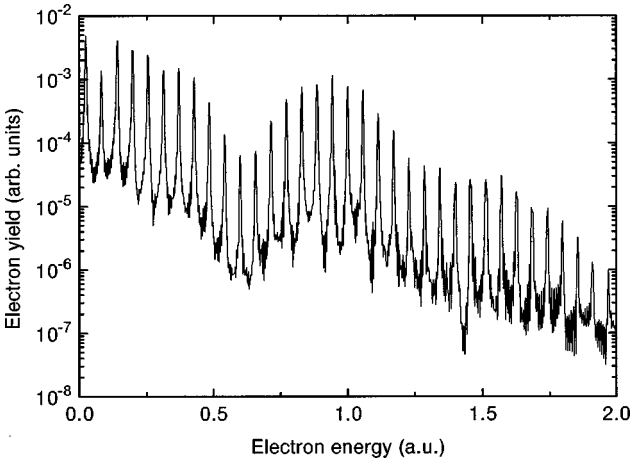

FIG. 1. Calculated ATI spectrum of argon from the last ten cycles of a 19-cycle flat-top pulse with peak field 0.044 a.u. at 800 nm, along the polarization vector. At this intensity there is maximum enhancement of the ATI peaks around 25 eV, leading to a very pronounced plateau in this logarithmic plot.

III. RESULTS AND DISCUSSION

A. Electron spectra

Simulations were run with a 19-cycle pulse, i.e., a 9-cycle leader with the absorber starting at a distance of 60 bohrs, followed by a collection period during which the absorber was gradually moved out to a distance of 1540 bohrs. This was done for intensities corresponding to peak electric fields E_0 ranging from 0.02 to 0.075. At this latter intensity, the tunneling yield has increased to about 3% per cycle [30], so that significant depletion already takes place during the 19-cycle pulse. For still higher intensities, it therefore seems that pulse-shape effects would start to dominate the results, and the analysis of the results as an intensity-dependent ionization rate will become questionable. At the very low intensities, ionization is expected to be dominated by very narrow (long-lived) Rydberg resonances, requiring much longer pulses before a steady ionization rate is reached.

Figure 1 shows a typical electron spectrum resulting from the simulation procedure, containing peaks up to 45 eV (faster electrons are at least partly absorbed at the far end of the grid). For the intensity shown (68 TW/cm^2), the spectrum displays a pronounced plateau around 25 eV. At 5% higher or lower intensities, the corresponding peaks shrink an order of magnitude, showing that the plateau is due to a resonance. This behavior closely resembles high-order enhancements (HOEs) observed in experiments [10,16]. At low intensities, the width of the calculated ATI peaks is completely due to the short (10-cycle) interval over which the electron production is analyzed (and to the width of the analysis filter, which is adapted to this): the natural width can be deduced from the rate of decrease of the ground-state population, and would be several orders of magnitude smaller. This rate roughly behaved as $\exp(220E_0)$, and thus increases by nearly four or-

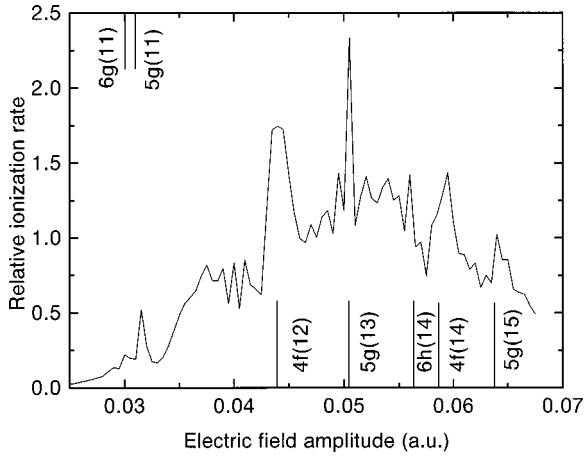

FIG. 2. Ionization rate in a 19-cycle laser pulse, divided by the average trend e^{220E} to make representation on a linear scale possible. Expected positions of various resonances are indicated, but their effect on the total rate seems to be limited to an enhancement of about a factor 2.

ders of magnitude over the studied intensity range. This behavior is qualitatively different from, and greatly exceeds the Ammosov-Delone-Krainov rate [31] $6E_0^{-0.35}\exp(-0.83/E_0)$, which is not surprising since we are not in the tunneling regime. From the total ionization rate as a function of intensity (Fig. 2), it can be seen that resonances only have a minor effect on the total decay rate (a factor 2 is already exceptional), although they do cause pronounced variation in the production of high-energy electrons.

The ponderomotive energy increases over the intensity range studied from 0.5 to 7 photon energies. In an experiment, this would make the order of a specific resonance peak (i.e., the number of photons absorbed to create those electrons) ambiguous. Since each simulation employs a unique intensity, it is possible to monitor the ionization process of a given order as it scans through resonances at several different numbers of photons, without contamination from production of other orders at different intensities. The partial ATI yields of some representative peaks, obtained by integrating the ATI peaks in a $0.3\hbar\omega$-wide interval around their nominal position, are shown in Fig. 3. The higher-order peaks show several high-contrast resonance enhancements.

The procedure sketched above is not able to bring out the Rydberg resonances that dominate the low-energy part of the ATI spectrum, because the leader is too short to develop them. In addition, the higher Rydberg states (above $n=6$), are too large to fit on the initial grid. To study such resonances in detail, another series of simulations was done, in which a leader of 30 cycles was used and the initial position of the absorber was moved out to 140 bohrs. This is enough to contain states up to $n=8$. With these parameters, the intensity was varied around the 11-, 12-, and 13-photon resonance with the threshold, in steps small enough to resolve the expected Rydberg resonances.

This procedure indeed nicely reveals a set of very narrow resonances, shown in Fig.4. The 11-photon resonant region is rather uneventful, and shows a single series of resonances, at the positions expected for ponderomotively shifting, quantum-defectless Rydberg states of principal quantum numbers $n=5$ and higher. Based on selection rules for pho-

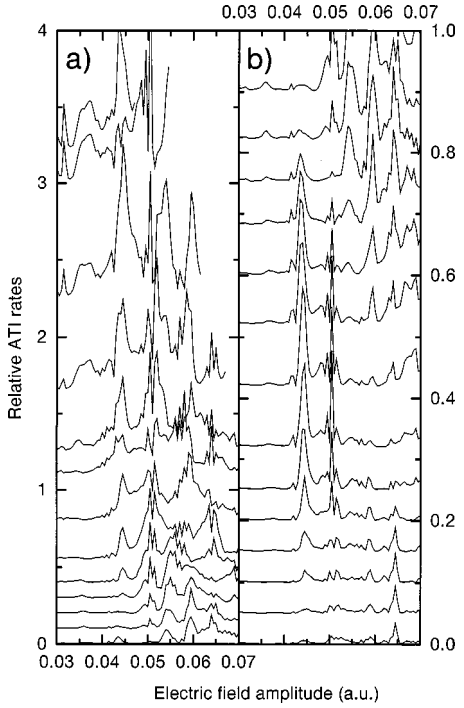

FIG. 3. Partial yield of the individual ATI channels as a function of the field amplitude, divided by e^{220E} to take out the huge overall increase of rates with intensity, and thus make representation on a linear scale possible. The curves are offset from each other for clarity; in reality they all approximately hit zero at their lowest point. In (a) the lower-order channels are plotted, from 13-photon ionization (top) to 25-photon ionization (bottom). In (b) the higher orders, from the 23-photon (top) to 37-photon (bottom) channel, are plotted. Note the different vertical scales of (a) and (b). Especially in the high-order spectrum the signal is almost exclusively due to narrow resonances, each resonance enhancing a comparatively small range of neighboring channels.

ton absorption, these resonances should be caused by even-parity states. The absence of a peak at the $n=4$ position suggests that these resonances are caused by g states, rather than s or d states. In fact, the apparent absence of resonances due to these lower angular-momentum states (which should be distiguishable by their quantum defect) is conspicuous. The enhancement caused by the g states is very prominent in the first few ATI orders, but hardly visible at higher electron energies.

In the 12-photon region, the situation is more diverse. The low-order ATI spectrum shows a number of very narrow resonances, which do not seem to correlate (and sometimes even anticorrelate) with a series of broader resonances in the high-order part. For instance, at $E=0.041$ a very pronounced enhancement in the 15-photon signal coincides with a minimum in the 28-photon peak. At the slightly higher intensity, $E=0.044$, the situation is reversed. Apparently this resonant state mainly decays by backscattering, producing a pronounced plateau.

In an earlier paper [16] we compared our numerical results with the experimental spectra of Hertlein *et al.* [10], by directly adding the (low-resolution) electron spectra calculated at different intensities, weighted by a factor resembling the intensity distribution in a three-dimensional Gaussian focus. A much higher resolution can be extracted from the

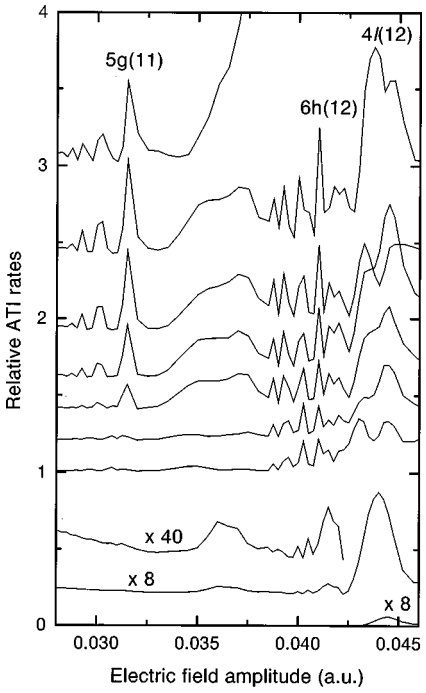

FIG. 4. Partial yield of various ATI channels as a function of field amplitude E, divided by e^{220E}. From top to bottom we see the channels due to 12−18-, 28- (twice), and (partially shown) 30-photon ionization. The latter two are magnified vertically by a factor 8 with respect to the first seven. The low-order traces show enhancement by resonances with Rydberg series at the 11- and 12-photon level, as well as a broad structure in between. The 28-photon channel, representative for the primary plateau region, is dominated by the enhancement at $E=0.044$; its low-intensity part is further enlarged to show the the two weaker enhancements. Note that the high-order enhancements do not line up very well with the strongest peaks in the low-order spectrum. The peak marked $4l$ seems a barely resolvable doublet in low order. The doublet coalesces into a single narrower structure in the plateau, although only the right member of the doublet seems to contribute at the 30-photon level.

same simulation runs by realizing that the yield vs field curves in Fig. 3 can be translated into an electron spectrum (yield vs energy) by making use of the ponderomotive shift of the ionization potential, which makes electrons of a single order appear at an intensity-dependent energy. In this case the resolution is determined by the total pulse duration, including the leader, and not limited by the duration of the collection period or the size of the spatial grid. To turn the yield curves into a spectrum, one thus simply multiplies the yield by the focal intensity distribution function, and relabels the horizontal axis [in an order-dependent way: $U=N\hbar\omega-U_0-U_p(I)$]. The total electron spectrum is then obtained by adding the single-order electron spectra for all orders. Figure 5 shows the result at a number of selected focal peak intensities. It can be seen that the high-order enhancement observed by Hertlein *et al.* actually stays prominent over a wide range of intensities, the growth of the volume in which it is excited making up for the much higher total ionization yield of the later HOEs. Typically HOEs have ATI spectra that are sharply delimited in order (the plateaus), sometimes even with a double-hump structure (Fig. 6).

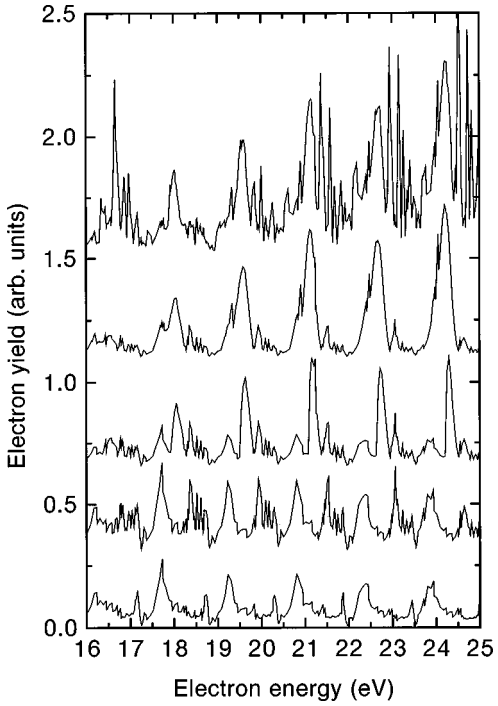

FIG. 5. Section of the high-order ATI spectrum averaged over the intensity distribution in a Gaussian focus, for focal peak fieds, intensities (a) 0.053 a.u., 99 TW/cm^2, (b) 0.046 a.u., 74 TW/cm^2, (c) 0.044 a.u., 68 TW/cm^2, (d) 0.0425 a.u., 63 TW/cm^2, and (e) 0.04 a.u., 56 TW/cm^2.

B. Wave-function analysis

To investigate the difference between resonances that lead to enhancements in the low-order part of the spectrum, and those that cause plateaus, we plotted the wave functions in the steady state that developed after the leader pulse [33]. Figure 7(b) shows that the low-order enhancement at a field of 0.0410 a.u. is caused by a state that circulates around the atom with a high angular momentum. Judging from the number of angular nodes it can be classified as an h state. Due to this high angular momentum it is apparently able to stay

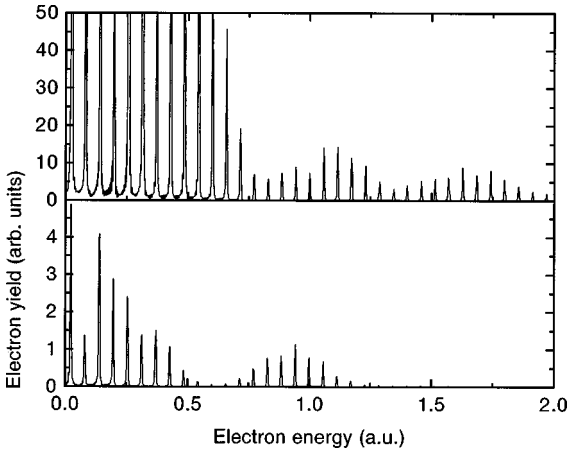

FIG. 6. Single-intensity ATI spectra at electric field amplitudes of (a) 0.065 and (b) 0.044 a.u., intensities for which strong enhancements in the high-order spectrum occur. The upper graph features a plateau with a double hump. Note that both traces are represented on a linear scale.

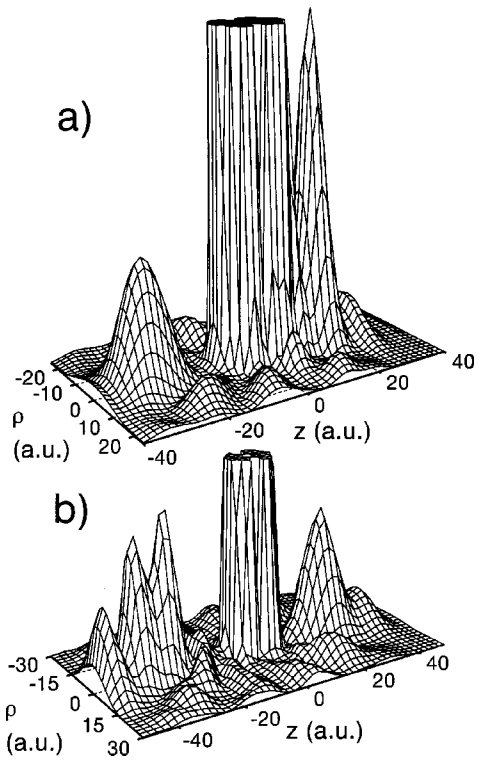

FIG. 7. The wave function after a steady state develops, for an electric field of (a) 0.0315 a.u. and (b) 0.041 a.u., 30° after the electric field peaks. Note the ring of population encircling the (strongly saturated) ground-state population. The population lobes in this ring are clearly visible where the plotting box cuts the wave function. The lobes might seem insignificant, but due to the cylindrical volume element they contain about as much population as the on-axis lobes. Four (a) or five (b) nodal planes radiate out from the nucleus to separate the lobes, identifying the states as a g and an h state, respectively.

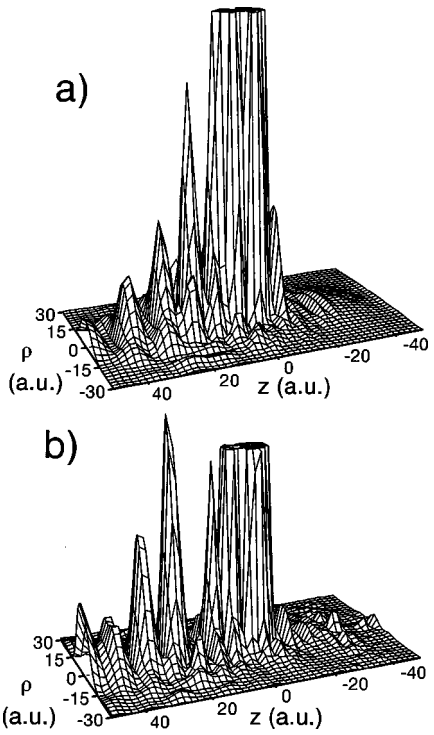

FIG. 8. Wave functions of resonances in the high-order ATI spectrum, at (a) $E=0.044$ and (b) $E=0.065$ a.u. The charge density consists of a number of bunches on the polarization (z) axis, which fly through the nucleus on each cycle, and cause plateaus on backscattering. These snapshots are taken near the time of maximum quiver displacement to the left; half a cycle earlier most of the population is on the right-hand side. Upon passing the nucleus part of it reflected, forming the high-momentum ripples visible on the right. Note that for these states there is only little population off axis. The ground-state population near the origin does not quiver, and strongly saturates on this scale.

away from the nucleus well enough to avoid collisions that result in large momentum transfer. (The inner turning point of $6h$ lies at $r=21>\alpha_0$.) A similar situation occurs for the 11-photon resonances with the g Rydberg series [Fig. 7(a)], which also causes enhancement only in the low-order channels. Their inner turning point is closer to the nucleus ($r\approx 14$ for $5g$), but at their resonant intensity the quiver amplitude α_0 is also smaller ($\alpha_0=E/\omega^2\approx 9.5$), so that the quiver motion cannot drive them against the nucleus. This is no longer true at the 13-photon resonance of the same states (for $5g$ this occurs near $E=0.05$, i.e., $\alpha_0\approx 15$), and indeed this resonance can be seen as a strong narrow spike in the high-order ATI peaks [Fig. 4(b)].

Wave packets tunneling out from under the saddle point are quite narrow in the direction perpendicular to the polarization vector. Due to the uncertainty relation this endows them with significant transverse momentum, which, at the distance at which they emerge out of the tunnel (around 12 bohrs) translates into a significant angular momentum. The position where the packets emerge also is at a good radial distance to overlap with Rydberg states of such angular momentum. If the phase of the emerging wave packet (controlled by the intensity-dependent energy of the ground state) is favorable, it interferes constructively with the wave function of the Rydberg population already present outside the barrier, and this greatly enhances the amount of population transfer through the barrier.

Figure 8 shows two resonant wave functions that cause a plateau; the population buildup around the atom here is mainly confined near the z axis, and the regions of enhanced electron density pass through the nucleus in the course of their quiver motion. Their multilobed structures are reminiscent of Kramers-Henneberger (KH) eigenstates in the dressed (time-averaged) atomic potential [34]. This situation is favorable for rescattering, and in the direction of polarization this is necessarily backscattering, leading to high momentum transfer. The multilobe nature of the KH states (which in itself is a consequence of the slow (axial) orbital motion of the electron within this state setting up a standing wave) favors some impact energies, and eliminates others, causing the modulations in the envelope of the high-order ATI spectrum characteristic of plateaus.

The overlap between the quivering KH states and the emerging tunneling packets is in general quite poor, since the quiver motion tends to move the KH states to the other side as where the packet is pulled out (the quiver motion is 180° out of phase with the electric field). A complicated mechanism of bunching and focusing [16] seems to be responsible for the population transfer in this case.

Wave functions like those in Fig. 8 are in general difficult to interpret, since the population that builds up due to the resonance is overlapped by the outward moving wave packets due to tunneling just before the field maximum. These wave packets also move along the polarization axis, and the overlap with the resonant population causes all kinds of rapidly moving interference structures. An attempt was made to get a better look at the quasistationary resonance charge distribution by removing the ground state somewhere during the pulse. The atom then stops emitting new wave packets. After a few cycles, earlier packets have moved off the grid, and this exposes the resonance population better, provided that it did not decay too much by ionization in the mean time.

This procedure only meets with limited success; some resonances decay very fast after the ground state has been removed, much faster than expected on the basis of their width as a function of intensity, so that hardly any population is left after the nonresonant packets are gone. This is remarkable in itself, and hints at the possibility that some resonances are stabilized by the presence of the ground state through destructive interference of their common decay channels (in a way similar to light-induced continuum structure [35]). Such a common decay could be the emission of low-energy electrons along the polarization axis; from the ground state such electrons appear from under the barrier near the field maxima, just at the same time as a quivering excited state might be driven against (and reflect from) this barrier from the outside, at very low energy.

In other cases, the remaining wave function does not behave in a quasistationary way. Sometimes, this could be ascribed to excitation of two resonances with nearly identical energy, the remaining difference leading to wave-function beats. The excitation process forces the phase of such slightly off-resonant states to stay in lockstep with the ground state, but after removal of the latter they start to evolve at their natural eigenfrequencies. In particular, this seems to occur for the strong high-order enhancement at $E=0.044$. The wave function seems to be built out of an on-axis component with two lobes, and a component with more off-axis activity. By slightly detuning the intensity, their relative importance can be tuned (although they will never be completely pure, since the resonance profiles overlap). Based on the number of ''angular'' nodal planes, the former component could be called a p state [36], and its excitation is favored in the high-intensity wing of the profile ($E=0.0444$). The latter then is an f state, better excited at $E=0.0433$. At both these frequencies an approximately quasiperiodic situation (with a population decay of about a factor 2.5 per cycle) is maintained for several cycles (Fig. 9).

The schizophrenic nature of this resonance is already indicated from the ATI spectra: low-order peaks seem to be split into two components. It is long since known that excitation in between two resonances might lead to destructive interference of their ionization, producing a deep notch in between them. At perturbative intensities this is quite common [37], since both excitation and ionization tend to be generated from the same spatial region of the wave function (near the nucleus), and the opposite detuning causes a relative phase difference of 180°. The novel effect in this case is that this notch turns into a strong maximum in the high-order spectrum. High-energy electrons can be generated only near

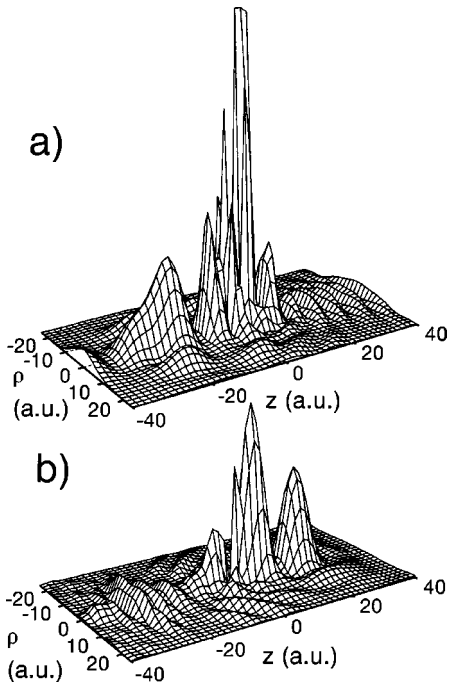

FIG. 9. Change in character of the resonant charge density on either side of the $4l$-resonance profile, as revealed after removal of the ground state and 2.5 cycles of propagation. The snapshots are taken near the time of the electric field maximum. At this time the quasistationary charge density is driven to one side of the nucleus, while backscattered decay products are escaping on the other side. This keeps the two components well separated, which facilitates interpretation of the plots. Function (b) is for $E=0.0433$ and shows a p-like state (the left lobe still in contact with the nucleus), while (a) is for $E=0.0444$ and has more f character, based on the off-axis lobes at $(\rho,z)=(12,-20)$ and $(14,-2)$. These lobes are actually rings due to the cylinder symmetry, and carry significant population (compare Fig. 7). Although (b) has some density off axis, this density is not stationary with respect to the quivering on-axis lobes, and does not show the pattern of nodal planes radiating out from the nucleus. Note that the two cases are viewed from opposing sides, in order to expose the relevant details optimally.

the origin of the Kramers-Henneberger frame, where high-energy impacts on the nucleus are possible, and this is a completely different place than where the state couples to the ground state. Apparently, the relative phase of the two resonant wave functions there has flipped 180° compared to the point where they were initially excited, so that the interference in those high-energy ionization channels is now constructive. This then leads to an enhancement in between the resonances that is stronger than that of the individual resonances for those ATI orders to which they both would contribute. The accidental near degeneracy of two suitable resonances might thus be the reason why the plateau in argon is so much stronger than what has been observed in other noble gases.

Most features of the wave functions are only apparent on studying their full time history; this enables one to judge which features of the charge density are permanent, and which features are transient interferences due to overlap between wave packets of very different momentum. Such movies, together with a discussion on their interpretation, will be published elsewhere [38].

IV. CONCLUSIONS

It seems that strong resonance enhancement localized in the high-order part of the ATI spectrum is a quite common phenomenon, even at intensities where excited states are completely dynamic and the electron orbits are dominated by the quiver motion. In fact, virtually all superponderomotive electrons are due to such resonance processes. Resonant states can be classified into on-axis states that fly through the core at high speed each cycle, and high-angular-momentum states that orbit around the core and are only nudged slightly by it at their point of closest approach. The first class leads to the occurrence of plateaus in the high-order ATI spectrum, the envelope of which is an image of the on-axis probability density of the resonant state. The second class predominantly causes enhancement in the low-order ATI spectrum.

ACKNOWLEDGMENT

This work was supported by the FOM (Foundation for Research on Matter), which is subsidized by NWO (Netherlands Organization for the Advancement of Research).

APPENDIX: THE PROPAGATION ALGORITHM

The calculation is performed in the velocity gauge. Because the laser interaction in this gauge,

$$A(t)p = -iA(t)\left(\cos\vartheta\,\partial_r - \frac{\sin\vartheta}{r}\partial_\vartheta\right), \tag{A1}$$

contains a radial derivative as well as $\cos\vartheta$ dependence, it couples each grid point to eight neighbors. For efficiency reasons, only operations involving tridiagonal matrices are acceptable, and we use a Peaceman-Rachford-inspired split-operator scheme. Since in a tridiagonal matrix coupling with at most two neighbors is possible, the velocity-gauge Hamiltonian must split into (at least) four such matrices.

Apart from the atomic Hamiltonian $H^{\rm at}$ (purely radial) and the purely angular coupling $H^{\rm ang}$ due to $1/r\sin\vartheta\partial_\vartheta$, we chose to use the two mixed couplings H^+ and H^- (both due to $\cos\vartheta\partial_r$) that couple each odd angular momentum to the next lower even angular momentum, or the next higher one, respectively. In other words, the operator $\cos\vartheta$ is decomposed as $L^+ + L^-$, where L^+ raises the angular momentum of even-l states, and lowers that of odd-l states, and L^- does the reverse. Then $H^\pm = A(t)L^\pm\partial_r$.

For the propagation we used the scheme

$$\begin{aligned}(1-iH^{\rm ang}\tau)&(1-iH^+\tau/2)(1+iH^+\tau/2)^{-1}(1-iH^-\tau/2)\\ &\times(1+iH^-\tau/2)^{-1}(1-iH^{\rm at}\tau)(1+iH^{\rm at}\tau)^{-1}\\ &\times(1-iH^-\tau/2)(1+iH^-\tau/2)^{-1}(1-iH^+\tau/2)\\ &\times(1+iH^+\tau/2)^{-1}(1+iH^{\rm ang}\tau)^{-1},\end{aligned} \tag{A2}$$

which provides absolutely stable propagation, since, after the last factor combines with the first one of the next time step, it consists entirely of unitary pairs.

The radial derivative operators occurring in $H^{\rm at}$ and $H^\pm$ were approximated by an *implicit* finite-difference scheme (the Numerov and Simpson rule for the second and first derivative, respectively), which boosts the spatial order of the method to four, without significantly increasing the computational load per grid point (in particular, they preserve the tridiagonal nature of the required matrix-vector operations). Compared to the more commonly used length-gauge propagator [39], Eq. (A2) includes three times as many factors. The additional factors, due to $H^\pm$, can be implemented quite efficiently, though, since they are real and, being Toeplitz matrices, their factorizing into lower and upper triangular matrices for inversion can be done analytically [23].

[1] P. Agostini, F. Fabre, G. Mainfray, G. Petite, and N. K. Rahman, Phys. Rev. Lett. **42**, 1127 (1979).
[2] K. J. Schafer, B. Yang, L. F. DiMauro, and K. C. Kulander, Phys. Rev. Lett. **70**, 1599 (1993).
[3] G. G. Paulus, W. Nicklich, Huale Xu, P. Lambropoulos, and H. Walther, Phys. Rev. Lett. **72**, 2851 (1994).
[4] H. B. van Linden van den Heuvell and H. G. Muller, in *Studies in Modern Optics No. 8, Multiphoton Processes*, edited by S. J. Smith and P. L. Knight (Cambridge University Press, Cambridge, England, 1988).
[5] H. G. Muller, Comments At. Mol. Phys. **24**, 355 (1990).
[6] H. R. Reiss, Phys. Rev. A **22**, 1786 (1980).
[7] W. Becker, R. R. Schlicher, and M. O. Scully, J. Phys. B **19**, L785 (1986).
[8] P. Corkum, Phys. Rev. Lett. **71**, 1994 (1993).
[9] J. M. Schins, P. Breger, P. Agostini, R. C. Constantinescu, H. G. Muller, G. Grillon, A. Antonetti, and A. Mysyrowicz, Phys. Rev. Lett. **73**, 2180 (1994); Phys. Rev. A **52**, 1272 (1995).
[10] M. P. Hertlein, P. H. Bucksbaum, and H. G. Muller, J. Phys. B **30**, L197 (1997).
[11] P. Hansch, M. A. Walker, and L. D. Van Woerkom, Phys. Rev. A **55**, R2535 (1997).
[12] L.-A. Lompré, A. l'Huiller, P. Monot, M. Ferray, G. Mainfray, and C. Manus, J. Opt. Soc. Am. B **7**, 754 (1990).
[13] R. R. Freeman, P. H. Bucksbaum, H. Milchberg, S. Darack, D. Schumacher, and M. E. Geusic, Phys. Rev. Lett. **59**, 1092 (1987).
[14] At this intensity, the barrier is centered on $r=5$ bohrs, at a level of -11.5 eV.
[15] P. H. Bucksbaum, A. Sanpera, and M. Lewenstein, J. Phys. B **30**, L843 (1997).
[16] H. G. Muller and F. C. Kooiman, Phys. Rev. Lett. **81**, 1207 (1998).
[17] E. Cormier and P. Lambropoulos, J. Phys. B **29**, 1667 (1996).
[18] This ''gauge'' is a description in an oscillating frame, in which the radiative forces on the electron are cancelled by the inertial forces, and the only effect of the light is to make the position of the nucleus time dependent [W. C. Henneberger, Phys. Rev. Lett. **21**, 838 (1968)].
[19] P. A. Christiansen, Y. S. Lee, and K. S. Pitzer, J. Chem. Phys. **71**, 4445 (1979).
[20] J. L. Krause, K. J. Schafer, and K. C. Kulander, Phys. Rev. Lett. **68**, 3535 (1992); Phys. Rev. A **45**, 4998 (1992).
[21] C. E. Moore, *Atomic Energy Levels*, Natl. Bur. Stand. (U.S.)

No. 467 (U.S. GPO, Washington, DC, 1949), Vol. I, p. 212.
[22] This applies both to spin-orbit couplings and two-electron orbit-orbit couplings.
[23] H. G. Muller, Laser Phys. **9**, 138 (1999).
[24] The ionization rate of $m=\pm 1$ states was about two orders of magnitude smaller, and does not contribute to the ATI spectrum along the polarization vector, since it has a node there.
[25] This is a special case of the popular sine-square turn on in terms of the electric field $E(t)$.
[26] For instance, the atomic propagator evolves eigenstates with a frequency $\omega=(2/\Delta t)\arctan(E\Delta t/2)$, rather than with their eigenvalue E.
[27] R. Taïeb, V. Véniard, and A. Maquet, J. Opt. Soc. Am. B **13**, 363 (1996).
[28] M. J. Nandor, M. A. Walker, L. D. Van Woerkom, and H. G. Muller (unpublished).
[29] K. J. Schafer and K. C. Kulander, Phys. Rev. A **42**, 5794 (1990).
[30] This is the rate for a single orbital; even neglecting ionization from the p orbitals perpendicular to the polarization, the rate for the atom would be double.
[31] M. V. Ammosov, N. B. Delone, and V. P. Krainov, Zh. Eksp. Teor. Fiz. **91**, 2008 (1986) [Sov. Phys. JETP **64**, 1191 (1986)]; N. B. Delone and V. P. Krainov, Usp. Fiz. Nauk. **168**, 531 (1998) [Phys. Usp. **41**, 469 (1998)].
[32] In mathematical terms: the limit of a moving δ function cannot be taken pointwise.
[33] K. Im, R. Grobe, and J. H. Eberly, Phys. Rev. A **49**, 2853 (1994).
[34] M. Pont, N. R. Walet, M. Gavrila, and C. W. McCurdy, Phys. Rev. Lett. **61**, 939 (1988).
[35] Bonian Dai and P. Lambropulos, Phys. Rev. A **36**, 5205 (1987); P. L. Knight, M. A. Lauder, and B. J. Dalton, Phys. Rep. **190**, 1 (1990).
[36] This kind of identification should not be taken too literally: at some phases of the field the state is displaced so much that the nucleus is centered in one of the lobes, and at that moment the state has more s than p character.
[37] H. B. Bebb and A. Gold, Phys. Rev. **143**, 1 (1966).
[38] H. G. Muller, Opt. Express (to be published).
[39] K. C. Kulander, K. J. Schafer, and J. L. Krause, in *Atoms in Intense Laser Fields*, edited by M. Gavrila (Academic, New York, 1992), p. 247.